Er^{3+}-doped fluorogallate glass for mid-infrared applications

Tianfeng Xue (薛天锋), Liyan Zhang (张丽艳), Lei Wen (温 磊), Meisong Liao (廖梅松)*, and Lili Hu (胡丽丽)**

Shanghai Institute of Optics and Fine Mechanics, Chinese Academy of Sciences, Shanghai 201800, China
**Corresponding author: liaomeisong@siom.ac.cn;; **corresponding author: hulili@siom.ac.cn*
Received March 12, 2015; accepted May 15, 2015; posted online June 23, 2015

We report an Er^{3+}-doped fluorogallate glass with good thermal and chemical stability. The low maximum phonon energy and high mid-infrared (IR) transmittance of the glass are confirmed by Raman and IR spectra, respectively. Based on Judd–Ofelt theory, intensity parameters and radiative properties are determined from the absorption and emission spectra. The proposed glass possesses a large fluorescence branching ratio β (21.71%) and a maximum stimulated emission cross-section σ_{em} of Er^{3+}:$^4I_{11/2} \rightarrow {}^4I_{13/2}$ transition at 2.71 μm (1.04×10^{-20} cm^2). The results indicate that it can be potentially applied in high-power 2.7 μm fiber lasers.
OCIS codes: 160.4760, 160.0160, 160.5690, 260.3800, 160.2290, 140.3500.
doi: 10.3788/COL201513.081602.

Mid-infrared (IR) wavelength lasers, particularly fiber lasers at around 3 μm, have been used in numerous applications in a wide range of fields including military affairs, eye-safe laser radar, and medical surgery[1–4]. Because of the Er^{3+}:$^4I_{11/2} \rightarrow {}^4I_{13/2}$ transition at 2.7 μm, Er^{3+}-doped glass is especially attractive and has been investigated widely[3–31]. To obtain high-power output and high mid-IR laser efficiency, an appropriate glass host is extremely important. An efficient glass host must satisfy several important factors, such as high IR transmittance, low hydroxyl group (i.e., OH) concentration, low phonon energy, good thermal stability, and high rare-earth solubility.

Fluoride glass[3–10] presents low phonon energy and wide mid-IR transmittance. Er^{3+}-doped fluoride glasses have been used to develop fiber lasers around 2.8 μm. For example, output power of 10 W level at 2.8 μm was demonstrated by a heavily Er^{3+}-doped ZrF_4-BaF_2-LaF_3-AlF_3-NaF (ZBLAN) glass fiber laser in 1994[6]. In 2009, Tokita *et al.* reported a liquid-cooled 24 W mid-IR Er^{3+}: ZBLAN fiber laser[9]. In 2011, Faucher *et al.* reported fabrication of a 20 W passively cooled, single-mode, all-fiber laser at 2.8 μm from a heavily Er^{3+}-doped fluoride fiber[10]. However, the glass transition temperature (T_g) of ZBLAN is as low as 267°C[3], which means poor thermal stability. In addition, another disadvantage of ZBLAN is its poor chemical stability[4], and it is readily corroded in the moist environment. All these drawbacks limit the scaling up of the output power in laser applications. Consequently, researchers must find a new kind of mid-IR glass with better thermal and chemical stability.

Besides fluoride glass, studies on oxide system glass, such as tellurite[11], and germanate[12,13] glasses have been carried out. These traditional oxide glasses can be prepared and fiberized easily as they offer good thermal durability and stable physicochemical properties. However, these glasses possess high intrinsic phonon energy; for example, germanate glass possesses a maximum phonon energy of 900 cm^{-1}[13], and tellurite glass possesses a maximum phonon energy of 750 cm^{-1}[15]. The multiphonon relaxation rate depends on the maximum phonon energy of the host glass[5]. Compared with fluoride glass (500 cm^{-1})[3–6], the high phonon energy increases multiphonon relaxation rates in those glasses and reduces the quantum efficiency of lasers[5].

To obtain an advantageous glass host with both low phonon energy and high thermal stability, oxyfluoride glasses are expected to feature good optical and thermal properties representing a compromise between pure fluoride and oxide glasses. These glasses, such as fluorosilicate[16,17], fluorotellurite[18–22], and fluorophosphate[23,24], have been investigated over the last several years.

Gallium-based oxide glass possesses high thermal stability and relatively low phonon energy (650–675 cm^{-1})[32,33]; as such, this glass is a good candidate as glass host. In this work, a new kind of Er^{3+}-doped fluorogallate glass is prepared. A certain amount of fluorides is useful to remove OH^- in the glass via the reaction $F^- + OH^- \rightarrow HF\uparrow + O^{2-}$. Upon 980 nm excitation, an intense mid-IR emission at around 2.71 μm is observed. A large fluorescence branching ratio β (21.71%) and a maximum stimulated emission cross-section σ_{em} of Er^{3+}:$^4I_{11/2} \rightarrow {}^4I_{13/2}$ transition are obtained.

The investigated glass has the nominal composition $[35Ga_2O_3 - 45SrO - 10BaF_2 - 10(LaF_3 + YF_3 + AlF_3)] + xEr_2O_3$ ($x = 0$ and 5 mol. %, terms GaOF0 and GaOF5, respectively).

High-purity reagent grade chemicals were used as starting materials. The batches were weighed and dried in a vacuum dry chamber at 100°C for 1 h, and then transferred to a platinum crucible. Then the glass samples were melted at 1400°C in a furnace for 1 h and then poured into a preheated stainless steel mold. After annealing and optical polishing, a series of measurements were performed at room temperature. The refractive indices of the samples

 © 2015 Chinese Optics Letters

were measured by the prism minimum-deviation method, and the values for GaOF0 and GaOF5 are 1.7190 and 1.7394, respectively. Using distilled water as an immersion liquid, the densities were measured by Archimedes' method. Characteristic temperatures were determined using a NETZSCH STA 409PC/PG instrument. IR transmission spectra were obtained by a Thermo Nicolet [Nexus Fourier-transform (FT) IR] spectrophotometer. Raman spectra were recorded with a Renishaw inVia Raman spectrometer using a 488 nm excitation line. A Perkin–Elmer Lambda 900 UV/visible/near-IR (NIR) spectrophotometer was used to measure absorption spectrum in the 250–1700 nm region. Emission spectra were measured by a Triax 550-type spectrometer (Jobin–Yvon) upon excitation at 980 nm.

The chemical durability of the GaOF5 sample was measured as follows. First, the weighed sample (W1) was placed in distilled water. The glass was then kept in a thermostatic water bath at 95°C for 24 h, after which the sample was cooled and dried in a drying box at 60°C for 4 h. Finally, the dry sample was weighed again (W2). The chemical durability of GaOF5 glass sample was evaluated in terms of the ΔW value, which was calculated as follows[21]

$$\Delta W = \frac{\mathrm{W1} - \mathrm{W2}}{\mathrm{W1}} \times 100\%. \tag{1}$$

The ΔW of GaOF5 is 75.0 mg/g; this value is approximately half of that of ZBLAN glass (151.6 mg/g)[21]. As a result, GaOF5 exhibits stronger resistance to water corrosion compared with ZBLAN glass.

The temperature of glass transition T_g and temperature of onset crystallization peak T_x are determined using a NETZSCH STA 409PC/PG differential scanning calorimeter at a heating rate of 10 K/min. A higher T_g endows glass with good thermal stability at high pumping intensities[31]. The difference between T_g and T_x, $\Delta T = T_x - T_g$, is frequently quoted as a rough indicator of thermal stability[20,21]. A large ΔT means strong inhibition to crystallization. Since fiber drawing has a reheating process and any crystallization during this process will enhance the scattering loss of the fiber, it is desirable for a glass to have ΔT as large as possible. Terms T_g and ΔT of GaOF5 are 640°C and 150°C, respectively; these values are much higher than ZBLAN glass without Er^{3+} (T_g:267°C, ΔT:93°C)[3]. Therefore, GaOF5 is probably more easily drawn into fibers than ZBLAN.

The Raman spectrum of the host glass is shown in Fig. 1. Peaks are located at 254, 518, and 671 cm^{-1}. The low-frequency peaks at 254 cm^{-1} affirms the collective modes of local structures and heavy-metal vibrational modes[32]. The band at 671 cm^{-1} is attributed to the stretching vibration of nonbridging oxygen in [GaO_4] tetrahedral[32,33] and the band at 518 cm^{-1} can be attributed to Ga-O-Ga bond vibrations between two [GaO_4] tetrahedra[33]. The maximum phonon energy of GaOF0 is 671 cm^{-1}, which is lower than those of some glass systems, such as

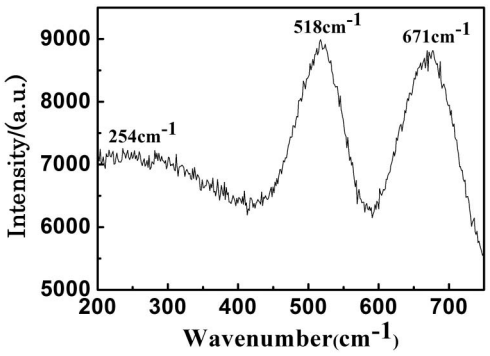

Fig. 1. Raman spectrum of GaOF0 sample at room temperature.

germanate (900 cm^{-1})[13], tellurite (750 cm^{-1})[15], and fluorotellurite (700 cm^{-1})[22]. The energy gap between the Er^{3+}:$^4I_{11/2} \rightarrow {}^4I_{13/2}$ transition is approximately 3680 cm^{-1}, which is over 5 times the maximum phonon energy of our glass. Thus, nonradiative relaxation induced by multiphonon excitation (W_{mp}) is minimal, and its effects on laser performance may be ignored[5,16].

Figure 2 shows the transmittance spectrum of 1 mm thick GaOF0 which is used to determine the IR cutoff wavelength and OH absorption of the glass. The IR cutoff wavelength is the wavelength which the transmission of a 1 mm thick sample is 10%[34]. The IR cutting edge of GaOF0 glass extends to 6.8 μm, which indicates that the investigated glass is a good kind of mid-IR material. The OH^- concentration in the glass can be expressed by[7]

$$\alpha_{\mathrm{OH}} = \ln(T/T_0)/l, \tag{2}$$

where l is the thickness of the sample; T and T_0 are the incident and transmitted intensities, respectively. The calculated absorption coefficient α_{OH} at 3.14 μm is 0.07 cm^{-1}. In general, the OH absorption band extends from 2500 to 3800 cm^{-1} because of fundamental stretching vibrations of the OH groups; this region involves the energy gap of Er^{3+}:$^4I_{11/2} \rightarrow {}^4I_{13/2}$ (~3680 cm^{-1}). Therefore, decreasing OH contents can enhance the 2.7 μm emission. The

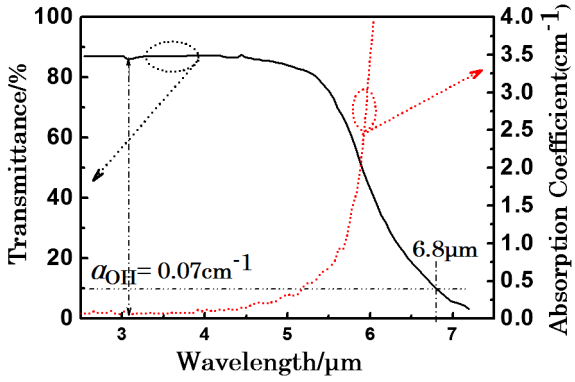

Fig. 2. Transmittance spectrum and the calculated absorption spectrum of GaOF0 at room temperature.

OH in GaOF glass may be further decreased if the melting conditions are improved. Additional studies on OH removal in this glass will be carried out in the future.

Figure 3 shows the absorption spectrum of GaOF5 sample at room temperature. The shape and peak position of each transition are very similar to those in other Er^{3+}-doped glasses[3–31]. Absorption bands corresponding to transitions beginning from the ground state $^4I_{15/2}$ to the high levels $^4I_{13/2}$, $^4I_{11/2}$, $^4I_{9/2}$, $^4F_{9/2}$, $^2S_{3/2}$, $^2H_{11/2}$, $^4F_{7/2}$, $^4F_{5/2}$, $^4F_{3/2}$, $^2H_{9/2}$, $^4G_{11/2}$, and $^4G_{9/2}$ are labeled. The relative absorption at around 980 nm indicates that the glass can be excited efficiently by a 980 nm laser diode (LD). The inset of Fig. 3 shows the intense 2.71 μm emission spectrum of GaOF5 upon excitation at 980 nm.

Based on Judd–Ofelt (J–O) theory[35], the parameters Ω_t of Er^{3+}-doped glass can be calculated from a least-squares fit procedure to the integrated absorption bonds. The root-mean square error deviation of the intensity parameters is within 0.34×10^{-6}. This characteristic indicates the validity of J–O theory for predicting the spectral intensities of Er^{3+} and obtaining reliable calculations. As is shown in Table 1, Ω_2 in present glass is higher than that of ZBLAN, but lower than those of other glasses. In general, Ω_2 is associated with the covalency and asymmetry of the ligand field around the Er^{3+} ions[19]. This behavior suggests that the asymmetry of the site occupied by Er^{3+} and the covalency in fluorogallate glass are higher than those of ZBLAN, but lower than those of other glasses. Terms Ω_4 and Ω_6 are related to the rigidity and 6-s electron density of the Er^{3+}. As a spectroscopic quality factor, Ω_4/Ω_6 usually indicates the lasing efficiency of the laser transition of Er^{3+} in the host glass[19]. The relatively high Ω_4/Ω_6 value of the present glass will benefit the radiative transition (Table 1), which means a strong stimulated emission can be induced[19].

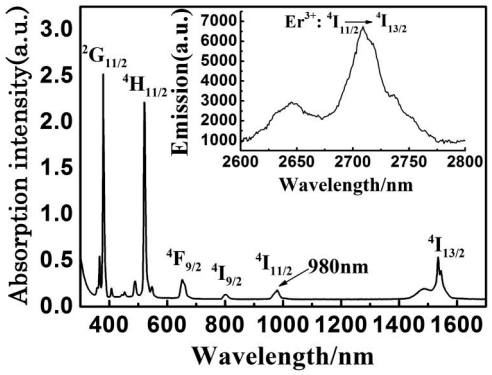

Fig. 3. Absorption spectrum of GaOF5 sample. Inset, 2.71 μm emission of GaOF5 at room temperature.

The spontaneous transition probability (A) and fluorescence branching ratio (β) of the transition Er^{3+}:$^4I_{11/2} \rightarrow {}^4I_{13/2}$ in various glasses are also listed in Table 1. The corresponding values for the GaOF5 are 25.89 s^{-1} and 21.71%, respectively. Compared with other glasses, GaOF5 has a relatively higher fluorescence branching ratio. The branching ratio is a critical parameter in laser design because it characterizes the possibility of attaining stimulated emission from specific transitions.

Based on Fuchtbauer–Ladenburg theory[19], the stimulated emission cross section σ_{em} can be determined from the emission spectrum

$$\sigma_{em}(\lambda) = \frac{\lambda_p^4 A_{rad}}{8\pi c n^2} \times \frac{\lambda I(\lambda)}{\int \lambda I(\lambda) d\lambda}. \quad (3)$$

The absorption cross-section (σ_{abs}) can be calculated using the McCumber equation[19]

$$\sigma_{abs}(\lambda) = \sigma_{em}(Z_U/Z_L) \exp[(-\varepsilon - hc\lambda^{-1})/kT], \quad (4)$$

where λ_p is the peak fluorescence wavelength, A_{rad} is the spontaneous transition probability, $I(\lambda)$ is the fluorescence spectra intensity, and n and c are the refractive index and light velocity in vacuum, respectively. Term ε is the net free energy required to excite one Er^{3+} ion from the $^4I_{13/2}$ to $^4I_{11/2}$ state at the temperature T, and k and h are the Boltzmann's and Planck's constants, respectively. Terms Z_U and Z_L are the partition functions of the lower and upper manifolds, respectively.

The stimulated emission cross section and absorption cross section spectra obtained for GaOF5 are shown in Fig. 4(a), and the maximum value of σ_{em} is 1.04×10^{-20} cm^2. Compared with other glasses listed in

Table 1. J–O Intensity Parameters, Calculated Spontaneous Radiative Probability, Fluorescence Branching Ratio, and Calculated Emission Cross Section of Er^{3+}:$^4I_{11/2} \rightarrow {}^4I_{13/2}$ in Various Glasses

Glass	Ω_2 (10^{-20} cm^2)	Ω_4 (10^{-20} cm^2)	Ω_6 (10^{-20} cm^2)	Ω_4/Ω_6	A (s^{-1})	β (%)	σ_{em} (10^{-20} cm^2)	References
Fluoride (ZBLAN)	3.27	1.3	1.75	0.74	28.8	15.85	0.656	[4]
Fluorophosphate	5.14	1.02	0.91	1.12	22.16	17.63	0.657	[24]
Chalcohalide	6.37	1.41	0.73	1.93	48.4	16.6	0.66	[30]
Germanate	7.23	2.75	1.17	2.35	65.26	16.01	0.953	[36]
Tellurite	4.38	3.05	1.04	2.93	50.02	18.36	0.814	[36]
GaOF5	4.17	1.07	0.46	2.33	25.89	21.71	1.04	This work

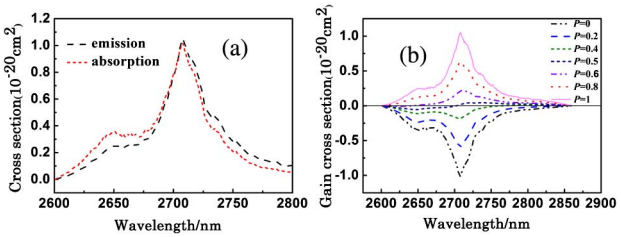

Fig. 4. (a) Calculated absorption and emission spectra corresponding to the Er^{3+}:$^4I_{11/2} \rightarrow {}^4I_{13/2}$ transition; (b) calculated gain cross-section with various P values ranging from 0 to 1 for the Er^{3+}:$^4I_{11/2} \rightarrow {}^4I_{13/2}$ transition of GaOF5.

Table 1, GaOF5 has a high emission cross section, which could provide high gain for a laser medium[37].

Based on σ_{em} and σ_{abs}, the wavelength dependence of net gain can be calculated[7] as a function of population inversion of the upper laser level to determine the gain property qualitatively

$$G(\lambda) = P \cdot \sigma_{em}(\lambda) - (1 - P) \cdot \sigma_{abs}(\lambda), \tag{5}$$

where P is the population inversion parameter, and σ_{em} and σ_{abs} are the emission and absorption cross section, respectively. The gain cross section of GaOF5 as a function of population inversion is shown in Fig. 4(b). A positive gain is achieved when $P > 0.5$, close to the case in ZBLAN glass[38], which implies that a low pumping threshold could be achieved during Er^{3+}:$^4I_{11/2} \rightarrow {}^4I_{13/2}$ laser operation.

As usual, the experimental lifetime (τ_{exp}) in the glass is lower than the calculated value (τ_{rad}) based on the J–O theory and the deviation is due to the nonradiative decay rates. Term τ_{exp} can be defined as[39]

$$\frac{1}{\tau_{exp}} = \frac{1}{\tau_{rad}} + W_{mp} + W_{cq} + W_{et} + W_{OH}, \tag{6}$$

where the terms W_{mp}, W_{cq}, W_{et}, and W_{OH} denote the nonradiative decay rates corresponding to the multiphonon relaxation, concentration quenching, energy transfer to another doping impurity, and hydroxyl groups, respectively.

As we have previously analyzed in this work, the multiphonon relaxation for Er^{3+}:$^4I_{11/2} \rightarrow {}^4I_{13/2}$ transition is minimal because of the low maximum phonon energy. Therefore, the W_{mp} can be ignored. All the starting materials are high-purity reagent-grade chemicals, so W_{et} induced by the impurity can also be neglected in the present glass. The intense emission at 2.71 μm means low concentration effects in the present glass which means that W_{cq} is very small.

Hydroxyl groups play a dominate role in the nonradiative decay process for 2.7 μm emission. We consider that the main nonradiative decay in our glass is due to W_{OH}, and it will be further decreased if we improve the melting condition. Then the deviation between τ_{exp} and τ_{rad} will be small. The quantum efficiency η, which is defined as the ratio of τ_{exp} and τ_{rad}, will be expected to be a high value.

In conclusion, a new kind of Er^{3+}-doped fluorogallate glass with low maximum phonon energy is prepared. Compared with fluoride glass, the proposed glass possesses better chemical stability, higher T_g (640°C) and larger ΔT (150°C), and all of these characteristics are suitable for the fabrication of high-power laser fiber. A large fluorescence branching ratio ($\beta = 21.71\%$) and stimulated emission cross-section ($\sigma_{em} = 1.04 \times 10^{-20}$ cm^2) at 2.71 μm are obtained by J–O theory. In addition, the nonradiative relaxation at 2.7 μm in the glass is also discussed. The results suggest that the proposed glass might be considered as a promising material for mid-IR high-power fiber lasers.

This work was supported by the Hundred Talents Program of the Chinese Academy of Sciences, the National Natural Science Foundation of China (Nos. 61475171 and 61177083), the Pujiang Talent Plan (No. 14PJ1409200), and the Joint Research Project of Chinese Academy of Science and Japan Society for the Promotion of Science (No. GJHZ1412)

References

1. M. D. Sario, L. Mescia, F. Prudenzano, F. Smektala, F. Deseveday, V. Nazabal, J. Troles, and L. Brilland, Opt. Laser Technol. **41**, 99 (2009).
2. S. Li, P. Wang, H. Xia, J. Peng, L. Tang, Y. Zhang, and H. Jiang, Chin. Opt. Lett. **12**, 021601 (2014).
3. K. Ohsawa and T. Shibata, J. Lightwave Technol. **2**, 602 (1984).
4. F. Huang, X. Liu, L. Hu, and D. Chen, Sci. Rep. **4**, 5053 (2014).
5. Y. Tian, R. Xu, L. Hu, and J. Zhang, Opt. Mater. **34**, 308 (2011).
6. Ch. Frerichs, Int. J. Infrared Millimeter Waves **15**, 635 (1994).
7. F. Huang, Y. Guo, Y. Ma, L. Zhang, and J. Zhang, Appl. Opt. **52**, 1399 (2013).
8. F. Huang, X. Liu, W. Li, L. Hu, and D. Chen, Chin. Opt. Lett. **12**, 051601 (2014).
9. S. Tokita, M. Murakami, S. Shimizu, M. Hashida, and S. Sakabe, Opt. Lett. **34**, 3062 (2009).
10. D. Faucher, M. Bernier, G. Androz, N. Caron, and R. Vallée, Opt. Lett. **36**, 1104 (2011).
11. X. Fan, X. Wang, X. Li, K. Li, and L. Hu, Acta Opt. Sin. **34**, 0116001 (2014).
12. T. Wei, F. Chen, Y. Tian, and S. Xu, J. Quant. Spec. Radiat. Transfer **133**, 663 (2014).
13. R. Wang, Z. Yang, D. Zhou, Z. Song, and J. Qiu, J. Non-Cryst. Solids **383**, 200 (2014).
14. S. Jiang, T. Luo, B. C. Hwang, F. Smekatala, K. Seneschal, J. Lucas, and N. Peyghambarian, J. Non-Cryst. Solids, **236–264**, 364 (2000).
15. I. Jlassi, H. Elhouichet, S. Hraiech, and M. Ferid, J. Lumin. **132**, 832 (2012).
16. C. R. Kesavulu, V. B. Sreedhar, C. K. Jayasankar, K. Jang, D.-S. Shin, and S. S. Yi, Mater. Res. Bull. **51**, 336 (2014).
17. S. Xu, Z. Yang, S. Dai, J. Zhang, L. Hu, and Z. Jiang, J. Chin. Rare Earths **22**, 375 (2004).
18. R. Wang, X. Meng, F. Yin, Y. Feng, G. Qin, and W. Qin, Opt. Mater. Express **3**, 1127 (2013).
19. Y. Ma, Y. Guo, F. Huang, L. Hu, and J. Zhang, J. Lumin. **147**, 372 (2014).
20. H. Zhan, Z. Zhou, J. He, and A. Lin, Opt. Lett. **37**, 3408 (2012).
21. Y. Guo, G. Gao, M. Li, L. Hu, and J. Zhang, Mater. Lett. **80**, 56 (2012).

22. A. A. Assadi, K. Damak, R. Damak, R. Lachheb, A. Herrmann, E. Yousef, C. Rüssel, and R. Maâlej, J. Alloys Compd. **620**, 129 (2015).
23. L. Zhang, B. Yang, and L. Hu, J. Quant. Spec. Radiat. Transfer **147**, 47 (2014).
24. Y. Tian, R. Xu, L. Zhang, L. Hu, and J. Zhang, Opt. Lett. **36**, 109 (2011).
25. G. N. Merberg, Laser Surg. Med. **13**, 572 (1993).
26. A. Miguel, M. Al-Saleh, J. Azkargorta, R. Morea, J. Gonzalo, M. A. Arriandiaga, J. Fernandez, and R. Balda, Opt. Mater. **35**, 2039 (2013).
27. J. S. Javorniczky, P. J. Newman, D. R. MacFarlane, and D. R. MacFarlane, J. Non-Cryst. Solids **184**, 249 (1995).
28. F. Prudenzano, L. Mescia, L. Allegretti, M. D. Sario, F. Smektaka, V. Moizan, V. Nazabal, J. Troles, J. L. Doualan, G. Canat, J. L. Adam, and B. Boulard, Opt. Mater. **31**, 1292 (2009).
29. X. Li, X. Liu, L. Zhang, L. Hu, and J. Zhang, Chin. Opt. Lett. **11**, 121601 (2013).
30. H. Lin, A. Chen, Y. Yu, A. Yang, and Y. Wang, Opt. Lett. **36**, 1815 (2011).
31. M. Liao, T. Yamashita, L. Huang, Y. Arai, T. Suzuki, and Y. Ohishi, J. Non-Cryst. Solids **355**, 96 (2009).
32. K. Fukumi and S. Sakka, J. Non-Cryst. Solids **94**, 251 (1987).
33. K. Fukumi, T. Kokubo, K. Kamiya, and S. Sakka, J. Non-Cryst. Solids **84**, 100 (1986).
34. J. E. Shelby and R. M. Slilaty, J. Appl. Phys. **68**, 3207 (1990).
35. G. S. Ofelt, J. Chem. Phys. **37**, 511 (1962).
36. Y. Guo, Y. Tian, L. Zhang, L. Hu, and J. Zhang, J. Non-Cryst. Solids **377**, 119 (2013).
37. T. Wei, Y. Tian, C. Tian, X. Jing, J. Zhang, L. Zhang, and S. Xu, Opt. Mater. Express **4**, 2150 (2014).
38. B. Wang, L. Cheng, H. Zhong, J. Sun, Y. Tian, X. Zhang, and B. Chen, Opt. Mater. **31**, 1658 (2009).
39. K. U. Kumar, P. Babu, K. H. Jang, H. J. Seo, C. K. Jayasankar, and A. S. Joshi, J. Alloys Compd. **458**, 509 (2008).